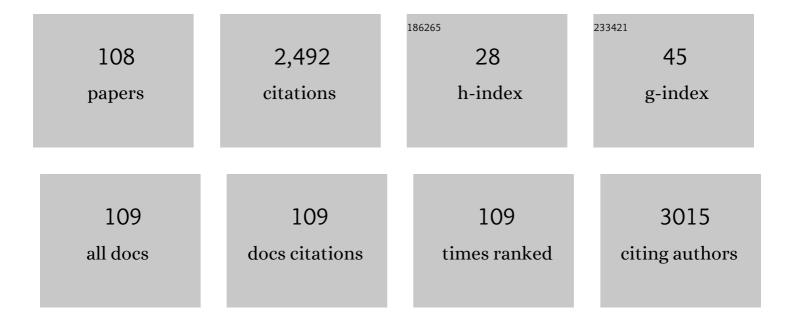


List of Publications by Year in descending order

Source: https://exaly.com/author-pdf/4883909/publications.pdf Version: 2024-02-01



OI FENC

#	Article	IF	CITATIONS
1	Structure of synthetic Na-birnessite: Evidence for a triclinic one-layer unit cell. American Mineralogist, 2002, 87, 1662-1671.	1.9	152
2	Single Nanocrystals of Anatase-Type TiO ₂ Prepared from Layered Titanate Nanosheets: Formation Mechanism and Characterization of Surface Properties. Langmuir, 2007, 23, 11782-11790.	3.5	152
3	Synthesis of Crystal-Axis-Oriented BaTiO3 and Anatase Platelike Particles by a Hydrothermal Soft Chemical Process. Chemistry of Materials, 2001, 13, 290-296.	6.7	144
4	Facile Formation of Anatase/Rutile TiO2 Nanocomposites with Enhanced Photocatalytic Activity. Molecules, 2019, 24, 2996.	3.8	142
5	Growth fusion of submicron spherical boron carbide particles byÂrepetitive pulsed laser irradiation in liquid media. Applied Physics A: Materials Science and Processing, 2010, 99, 797-803.	2.3	74
6	Hydrothermal synthesis of layered hydroxide zinc benzoate compounds and their exfoliation reactions. Journal of Materials Chemistry, 2006, 16, 474-480.	6.7	65
7	Ferroelectric Mesocrystalline BaTiO ₃ /SrTiO ₃ Nanocomposites with Enhanced Dielectric and Piezoelectric Responses. Chemistry of Materials, 2015, 27, 4983-4994.	6.7	62
8	Topotactic Transformation Reaction from Layered Titanate Nanosheets into Anatase Nanocrystals. Journal of Physical Chemistry C, 2009, 113, 20275-20280.	3.1	61
9	Modification of TiO ₂ Electrode with Organic Silane Interposed Layer for High-Performance of Dye-Sensitized Solar Cells. ACS Applied Materials & Interfaces, 2014, 6, 5818-5826.	8.0	52
10	Ti-O-O coordination bond caused visible light photocatalytic property of layered titanium oxide. Scientific Reports, 2016, 6, 29049.	3.3	50
11	Transformation of potassium Lindquist hexaniobate to various potassium niobates: solvothermal synthesis and structural evolution mechanism. Dalton Transactions, 2013, 42, 7699.	3.3	48
12	Synthesis of [111]- and {010}-faceted anatase TiO ₂ nanocrystals from tri-titanate nanosheets and their photocatalytic and DSSC performances. Nanoscale, 2015, 7, 7980-7991.	5.6	48
13	Hydrothermal Soft Chemical Synthesis and Particle Morphology Control of BaTiO3 in Surfactant Solutions. Journal of the American Ceramic Society, 2005, 88, 1415-1420.	3.8	47
14	Microwave-Assisted Topochemical Conversion of Layered Titanate Nanosheets to {010}-Faceted Anatase Nanocrystals for High Performance Photocatalysts and Dye-Sensitized Solar Cells. Crystal Growth and Design, 2014, 14, 5801-5811.	3.0	47
15	Single Crystal Growth of Birnessite- and Hollandite-Type Manganese Oxides by a Flux Method. Crystal Growth and Design, 2003, 3, 409-415.	3.0	45
16	Hydrothermal Syntheses of Layered Lithium Nickel Manganese Oxides from Mixed Layered Ni(OH)2â^'Manganese Oxides. Chemistry of Materials, 2002, 14, 3844-3851.	6.7	44
17	Solvothermal Soft Chemical Synthesis and Characterization of Nanostructured Ba _{1–<i>x</i>} (Bi _{0.5} 0.50.5) _{<i>x</i>} TiO ₃ Platelike Particles with Crystal-Axis Orientation. Chemistry of Materials, 2011, 23, 3978-3986.	6.7	42
18	Antiferroelectric Nature of CH3NH3PbI3â^'xClx Perovskite and Its Implication for Charge Separation in Perovskite Solar Cells. Scientific Reports, 2016, 6, 30680.	3.3	42

#	Article	IF	CITATIONS
19	Relationships between Cell Parameters of Dye-Sensitized Solar Cells and Dye-Adsorption Parameters. ACS Applied Materials & Interfaces, 2012, 4, 1928-1934.	8.0	41
20	Solvothermal soft chemical synthesis and characterization of plate-like particles constructed from oriented BaTiO3 nanocrystals. Journal of the Ceramic Society of Japan, 2010, 118, 141-146.	1.1	39
21	Ferroelectric Mesocrystals of Bismuth Sodium Titanate: Formation Mechanism, Nanostructure, and Application to Piezoelectric Materials. Inorganic Chemistry, 2013, 52, 10542-10551.	4.0	39
22	Photocatalytic and Dye-Sensitized Solar Cell Performances of {010}-Faceted and [111]-Faceted Anatase TiO ₂ Nanocrystals Synthesized from Tetratitanate Nanoribbons. ACS Applied Materials & Interfaces, 2014, 6, 16007-16019.	8.0	39
23	Fabrication of [100]-oriented bismuth sodium titanate ceramics with small grain size and high density for piezoelectric materials. Journal of the European Ceramic Society, 2014, 34, 1169-1180.	5.7	38
24	Mesocrystalline Nanocomposites of TiO ₂ Polymorphs: Topochemical Mesocrystal Conversion, Characterization, and Photocatalytic Response. Crystal Growth and Design, 2015, 15, 1214-1225.	3.0	38
25	Bismuth chalcogenide iodides Bi ₁₃ S ₁₈ I ₂ and BiSI: solvothermal synthesis, photoelectric behavior, and photovoltaic performance. Journal of Materials Chemistry C, 2020, 8, 3821-3829.	5.5	38
26	Preparation of Crystalâ€Axisâ€Oriented Barium Calcium Titanate Plateâ€Like Particles and Its Application to Oriented Ceramic. Journal of the American Ceramic Society, 2011, 94, 3716-3721.	3.8	30
27	Antiferroelectric-to-Ferroelectric Switching in <mml:math xmlns:mml="http://www.w3.org/1998/Math/MathML" display="inline"><mml:mrow><mml:msub><mml:mrow><mml:mi>CH</mml:mi></mml:mrow><mml:mrow><mu and Its Potential Role in Effective Charge Sepa. Physical Review Applied. 2016. 6.</mu </mml:mrow></mml:msub></mml:mrow></mml:math 	ml:ສຳ8>3 </td <td>/mml:mn></td>	/mml:mn>
28	Recent progress in piezoelectric thin film fabrication <i>via</i> the solvothermal process. Journal of Materials Chemistry A, 2019, 7, 16046-16067.	10.3	30
29	Dye-sensitized solar cells based on anatase TiO2 nanocrystals exposing a specific lattice plane on the surface. Applied Physics Letters, 2010, 97, 131906.	3.3	28
30	Hydrothermal synthesis and formation mechanism of the anatase nanocrystals with co-exposed high-energy {001}, {010} and [111]-facets for enhanced photocatalytic performance. RSC Advances, 2017, 7, 24616-24627.	3.6	28
31	Synthesis of {010}-faceted anatase TiO ₂ nanoparticles from layered titanate for dye-sensitized solar cells. CrystEngComm, 2014, 16, 8885.	2.6	27
32	In Situ Photochemical Surface Passivation of CdSe/ZnS Quantum Dots for Quantitative Light Emission and Enhanced Photocurrent Response in Solar Cells. Journal of Physical Chemistry C, 2014, 118, 2178-2186.	3.1	25
33	Soft chemical in situ synthesis, formation mechanism and electrochemical performances of 1D bead-like AgVO ₃ nanoarchitectures. Journal of Materials Chemistry A, 2015, 3, 18127-18135.	10.3	25
34	Removal of trace arsenic to below drinking water standards using a Mn–Fe binary oxide. RSC Advances, 2017, 7, 1490-1497.	3.6	23
35	Microwave assisted hydrothermal synthesis of tin niobates nanosheets with high cycle stability as lithium-ion battery anodes. Chinese Chemical Letters, 2019, 30, 771-774.	9.0	22
36	Interplay between Dye Coverage and Photovoltaic Performances of Dye-Sensitized Solar Cells Based on Organic Dyes. Journal of Physical Chemistry C, 2014, 118, 20184-20192.	3.1	21

#	ARTICLE {0001} and {10 <mml:math <="" th="" xmlns:mml="http://www.w3.org/1998/Math/MathML"><th>IF</th><th>CITATIONS</th></mml:math>	IF	CITATIONS
37	altimg="si1.svg"> <mml:mover accent="true"><mml:mrow><mml:mn>1</mml:mn></mml:mrow><mml:mrow><mml:mo stretchy="false">Â⁻</mml:mo </mml:mrow>1} facet heterojunctions on hexagonal pyramid CdS single crystals with high photoactivity and photostability for hydrogen</mml:mover 	12.7	20
38	Anomalous piezoelectric response of ferroelectric mesocrystalline BaTiO ₃ /Bi _{0.5} Na _{0.5} TiO ₃ nanocomposites designed by strain engineering. Nanoscale, 2018, 10, 8196-8206.	5.6	19
39	One-Dimensional Piezoelectric BaTiO ₃ Polycrystal of Topochemical Mesocrystal Conversion from Layered H ₂ Ti ₄ O ₉ ·H ₂ O Single Crystal. Crystal Growth and Design, 2018, 18, 7264-7274.	3.0	19
40	Microwave-Assisted Synthesis of High-Energy Faceted TiO2 Nanocrystals Derived from Exfoliated Porous Metatitanic Acid Nanosheets with Improved Photocatalytic and Photovoltaic Performance. Materials, 2019, 12, 3614.	2.9	19
41	Topochemical conversion of protonated titanate single crystals into platelike Ba _{0.5} Sr _{0.5} TiO ₃ mesocrystals with controllable microstructures. CrystEngComm, 2015, 17, 1758-1764.	2.6	18
42	Ferroelectric mesocrystalline BaTiO ₃ /BaBi ₄ Ti ₄ O ₁₅ nanocomposite: formation mechanism, nanostructure, and anomalous ferroelectric response. Nanoscale, 2019, 11, 3837-3846.	5.6	18
43	Raw Particle Aggregation Control for Fabricating Submicrometer-sized Spherical Particles by Pulsed-laser Melting in Liquid. Chemistry Letters, 2013, 42, 530-531.	1.3	17
44	Delithation, Exfoliation, and Transformation of Rock-Salt-Structured Li ₂ TiO ₃ to Highly Exposed {010}-Faceted Anatase. ACS Applied Materials & Interfaces, 2015, 7, 7995-8004.	8.0	17
45	Platelike Ag 2 Nb 4 O 11 mesocrystals: Soft chemical synthesis, formation mechanism and enhanced photocatalytic performance. Journal of Alloys and Compounds, 2016, 686, 48-54.	5.5	16
46	Synthesis of Anatase TiO ₂ Nanocrystals with Defined Morphologies from Exfoliated Nanoribbons: Photocatalytic Performance and Application in Dyeâ€sensitized Solar Cell. ChemistrySelect, 2019, 4, 4443-4457.	1.5	16
47	Facile Synthesis of {101}, {010} and [111]â€Faceted Anataseâ€TiO ₂ Nanocrystals Derived from Porous Metatitanic Acid H ₂ TiO ₃ for Enhanced Photocatalytic Performance. ChemistrySelect, 2018, 3, 2867-2876.	1.5	15
48	Electrostatic Self-Assembly Synthesis of Three-Dimensional Mesoporous Lepidocrocite-Type Layered Sodium Titanate as a Superior Adsorbent for Selective Removal of Cationic Dyes via an Ion-Exchange Mechanism. Langmuir, 2021, 37, 6080-6095.	3.5	15
49	A CdS/MnS p–n heterojunction with a directional carrier diffusion path for efficient photocatalytic H ₂ production. Inorganic Chemistry Frontiers, 2022, 9, 1100-1106.	6.0	15
50	Preparation of Nanoleaf-like Single Crystals of Anatase-type TiO2by Exfoliation and Hydrothermal Reactions. Chemistry Letters, 2006, 35, 1226-1227.	1.3	14
51	Topotactic synthesis and photocatalytic performance of one-dimensional ZnNb ₂ O ₆ nanostructures and one-dimensional ZnNb ₂ O ₆ /KNbO ₃ hetero-nanostructures. RSC Advances, 2014, 4, 56637-56644.	3.6	14
52	Topotactic soft chemical synthesis and photocatalytic performance of one-dimensional AgNbO3 nanostructures. Materials Letters, 2014, 137, 110-112.	2.6	14
53	Synthesis of {110}-faceted rutile TiO ₂ nanocrystals from tetratitanate nanoribbons for improving dye-sensitized solar cell performance. RSC Advances, 2016, 6, 9717-9724.	3.6	14
54	<i>In situ</i> topotactic synthesis of a porous network Zn ₂ Ti ₃ O ₈ platelike nanoarchitecture and its long-term cycle performance for a LIB anode. CrystEngComm, 2018, 20, 7329-7336.	2.6	14

#	Article	IF	CITATIONS
55	Oneâ€Pot Synthesis of [111]″{010} Facets Coexisting Anatase Nanocrystals with Enhanced Dye‧ensitized Solar Cell Performance. ChemistrySelect, 2016, 1, 6632-6640.	1.5	13
56	Ferroelectric mesocrystalline BaTiO3/Bi0.5K0.5TiO3 nanocomposites: Topochemical synthesis, enhanced piezoelectric and dielectric responses. Journal of Alloys and Compounds, 2020, 818, 152869.	5.5	13
57	Facile synthesis of TiO ₂ /Ag ₃ PO ₄ composites with co-exposed high-energy facets for efficient photodegradation of rhodamine B solution under visible light irradiation. RSC Advances, 2020, 10, 24555-24569.	3.6	12
58	Tetragonal Distortion of a BaTiO ₃ /Bi _{0.5} Na _{0.5} TiO ₃ Nanocomposite Responsible for Anomalous Piezoelectric and Ferroelectric Behaviors. ACS Omega, 2020, 5, 22800-22807.	3.5	12
59	Ni(OH)2 Nanosheets Modified Hexagonal Pyramid CdS Formed Type II Heterojunction Photocatalyst with High-Visible-Light H2 Evolution. ACS Applied Energy Materials, 0, , .	5.1	12
60	Strategy for Lowering Li Source Dosage While Keeping High Reactivity in Solvothermal Synthesis of LiMnO ₂ Nanocrystals. ACS Sustainable Chemistry and Engineering, 2013, 1, 570-573.	6.7	11
61	Controllable synthesis and morphology evolution from two-dimensions to one-dimension of layered K ₂ V ₆ O ₁₆ •nH ₂ O. CrystEngComm, 2015, 17, 3777-3782.	2.6	11
62	Topological relations and piezoelectric responses of crystal-axis-oriented BaTiO ₃ /CaTiO ₃ nanocomposites. RSC Advances, 2017, 7, 30807-30814.	3.6	11
63	Soft chemical synthesis and visible light photocatalytic performance of Ag@AgCl/H1.07Ti1.73O4 platelike composite with composition controlling. Journal of Alloys and Compounds, 2017, 727, 311-317.	5.5	11
64	BaTi4O9 mesocrystal: Topochemical synthesis, fabrication of ceramics, and relaxor ferroelectric behavior. Journal of Alloys and Compounds, 2019, 777, 335-343.	5.5	11
65	Bi ₁₃ S ₁₈ <i>X</i> ₂ -Based Solar Cells (<i>X</i> = Cl, Br, I): Photoelectric Behavior and Photovoltaic Performance. Physical Review Applied, 2021, 15, .	3.8	11
66	Enhanced Photovoltaic Performance of BiSCl Solar Cells Through Nanorod Array. ChemSusChem, 2021, 14, 3351-3358.	6.8	11
67	Hollow Square RodLike Microtubes Composed of Anatase Nanocuboids with Coexposed {100}, {010}, and {001} Facets for Improved Photocatalytic Performance. ACS Omega, 2020, 5, 14147-14156.	3.5	9
68	Tailored Hydrothermal Synthesis of Specific Facet-Dominated TiO ₂ Nanocrystals from Lepidocrocite-Type Layered Titanate Nanosheets: Systematical Investigation and Enhanced Photocatalytic Performance. Langmuir, 2020, 36, 4477-4495.	3.5	9
69	Synthesis and exfoliation of layered hydroxide zinc aminobenzoate compounds. Journal of the Ceramic Society of Japan, 2009, 117, 1115-1119.	1.1	8
70	Synthesis, Transformation Mechanism and Photocatalytic Properties of Various Morphologies Anatase TiO ₂ Nanocrystals Derived From Tetratitanate Nanobelts. ChemistrySelect, 2018, 3, 9953-9959.	1.5	8
71	Formation mechanisms and electrical properties of perovskite mesocrystals. Ceramics International, 2021, 47, 1479-1512.	4.8	8
72	Lithium Ion Battery Anode of Mesocrystalline CoTiO ₃ /TiO ₂ Nanocomposite with Extremely Enhanced Capacity. ACS Applied Energy Materials, 2021, 4, 13646-13656.	5.1	8

Qi Feng

#	Article	IF	CITATIONS
73	Electrochemical reaction mechanism of porous Zn2Ti3O8 as a high-performance pseudocapacitive anode for Li-ion batteries. Chinese Chemical Letters, 2022, 33, 4776-4780.	9.0	8
74	Synthesis of Lithiophorite with Sandwich Layered Structure by Hydrothermal Soft Chemical Process. Chemistry Letters, 1998, 27, 757-758.	1.3	7
75	Title is missing!. Journal of Materials Science Letters, 2003, 22, 999-1001.	0.5	7
76	Low Temperature Synthesis of BaTiO3 from Layered Titanate Nanosheet. Journal of the Ceramic Society of Japan, 2007, 115, 165-168.	1.3	7
77	Transformation of layered hydroxide zinc benzoate nanosheets into ZnO nanocrystals by electron beam irradiation. Journal of the Ceramic Society of Japan, 2008, 116, 657-660.	1.1	7
78	Structural and morphological evolution of an octahedral KNbO ₃ mesocrystal <i>via</i> self-assembly-topotactic conversion process. CrystEngComm, 2018, 20, 728-737.	2.6	7
79	Introduction of Fe ²⁺ in Fe _{0.8} Ti _{1.2} O ₄ ^{0.8â~`} nanosheets <i>via</i> photo reduction and their enhanced electrochemical performance as a lithium ion battery anode. Chemical Communications, 2019, 55, 186-189.	4.1	7
80	Synthesis of Layered Hydroxide Zinc <i>m</i> â€Aminobenzoate Compounds and Their Exfoliation Reactions. Chinese Journal of Chemistry, 2011, 29, 1837-1845.	4.9	6
81	Screening of Inorganic Adsorbents for Selective Adsorption of Thiophene from Model Gasoline. Separation Science and Technology, 2012, 47, 1926-1936.	2.5	6
82	Synthesis of Ba _x (Bi _{0.5} Na _{0.5}) _{1â^'x} TiO ₃ perovskite mesocrystals <i>via</i> a solvothermal topochemical process. CrystEngComm, 2019, 21, 3854-3862.	2.6	6
83	MoS ₂ -Modified CdS Hexagonal Pyramid To Form a New Photogenerated Carrier Migration Path with Highly Efficient Photocatalytic H ₂ Performance. Journal of Physical Chemistry C, 2022, 126, 9027-9033.	3.1	6
84	Hydrothermal soft chemical synthesis of BaTiO3 and titanium oxide with cocoon-like particle morphology. Journal of Materials Science, 2007, 42, 640-645.	3.7	5
85	Facile size-controllable synthesis process, bandgap blue shift, and enhanced photocatalytic performances of [111]-faceted anatase TiO ₂ nanocrystals. New Journal of Chemistry, 2017, 41, 10998-11008.	2.8	5
86	Hydrothermal synthesis and electrochemical performance of K0.8Fe0.8Ti1.2O4 as lithium ion battery anode. Materials Letters, 2019, 237, 145-148.	2.6	5
87	Rod-like incipient ferroelectric SrTiO3 polycrystal with crystal-axis orientation. Ceramics International, 2020, 46, 3675-3687.	4.8	5
88	Mesocrystalline effect in a NiTiO ₃ /TiO ₂ nanocomposite for enhanced capacity of lithium-ion battery anodes. Inorganic Chemistry Frontiers, 2022, 9, 2055-2067.	6.0	5
89	Synthesis of Sn2Nb2O7-GO nanocomposite as an anode material with enhanced lithium storage performance. Journal of Materials Science, 2020, 55, 3561-3570.	3.7	4
90	The Sn–C bond at the interface of a Sn2Nb2O7–Super P nanocomposite for enhanced electrochemical performance. New Journal of Chemistry, 2020, 44, 4478-4485.	2.8	4

#	Article	IF	CITATIONS
91	Remarkably enhanced ion-exchange capacity of H ₂ O ₂ -intercalated layered titanate. Chemical Communications, 2021, 57, 7394-7397.	4.1	4
92	Controllable preparation and formation mechanisms of BaTiO3/titanate nanocomposites from solvothermally synthesized K0.8Li0.27Ti1.73O4 crystal. Materials Chemistry and Physics, 2020, 249, 122964.	4.0	3
93	Electrochemical study of reduced graphene oxide@Zn2Ti3O8 nanocomposites as a superior anode for Li-ion battery. Chemical Engineering Science, 2022, 260, 117872.	3.8	3
94	Column Desulfurization of Hydrodesulfurized Gasoline Using Ce(IV)-Loaded Y-Zeolite Adsorbent. Journal of Chemical Engineering of Japan, 2012, 45, 324-330.	0.6	2
95	Controlling dye coverage instead of addition of organic acid to reduce dye aggregation in dye-sensitized solar cells. Solar Energy, 2020, 202, 507-513.	6.1	2
96	Development of Titania-supported Iridium Catalysts for the Acceptor-less Dehydrogenative Synthesis of Benzoxazoles. Journal of the Japan Petroleum Institute, 2021, 64, 271-279.	0.6	2
97	Soft Chemical Approach to Synthesis and Control of Functional Inorganic Materials. Journal of Ion Exchange, 2003, 14, 77-86.	0.3	2
98	Controllable preparation of two-dimensional oriented BaTiO3 polycrystals from K0.8Ti1.73Li0.27O4 crystals by a one-step solvothermal process. Ceramics International, 2022, 48, 10693-10703.	4.8	2
99	Improved dispersion ability of TiO2 nanoparticles for efficient dye-sensitized solar cells. Applied Surface Science, 2015, 357, 1658-1665.	6.1	1
100	Polymorphic Evolution of TiO ₂ in Hydrothermal Reaction System of Layered Titanate Nanosheets. ChemistrySelect, 2018, 3, 8703-8712.	1.5	1
101	Topochemical conversion of the discontinuous-zone-axis to form bismuth titanate oriented polycrystal nanocomposites. Inorganic Chemistry Frontiers, 2021, 8, 796-810.	6.0	1
102	Rapid Multialkylation of Aqueous Ammonia with Alcohols by Heterogeneous Iridium Catalyst under Simple Conditions. ChemCatChem, 2021, 13, 3588-3593.	3.7	1
103	The nonlinear optical properties of the nanohybrid thin film forming by intercalating methylene blue dye into layered titanate nanosheets. , 2011, , .		0
104	Hydrothermal Synthesis and Particle Morphology Control of K _{0.8} Li _{0.27} Ti _{1.73} O ₄ with Lepidocrocite-like Structure. Funtai Oyobi Fummatsu Yakin/Journal of the Japan Society of Powder and Powder Metallurgy, 2016, 63, 185-191.	0.2	0
105	Fabrication of Ba _{1â~x} Ca _x TiO ₃ Oriented Ceramics by Reactive Template Grain Growth Method Using Layered Titanate Template. Funtai Oyobi Fummatsu Yakin/Journal of the Japan Society of Powder and Powder Metallurgy, 2016, 63, 1009-1014.	0.2	0
106	SYNTHESES OF MIXED LAYERED NICKEL HYDROXIDE MANGANESE OXIDES BY HYDROTHERMAL INTERCALATION REACTION AND EXFOLIATION-RESTACKING HYDROTHERMAL REACTION. , 2002, , .		0
107	SYNTHESIS AND PARTICLE MORPHOLOGY CONTROL OF BaTiO3 AND TiO2 BY HYDROTHERMAL SOFT CHEMICAL PROCESS. , 2003, , .		0
108	In Situ Topochemically Converted 2-D BaTiO3 Polycrystals with Multifarious Zone Axes. Materials Advances, 0, , .	5.4	0